Iris recognition based on robust iris segmentation and image enhancement

Abhishek Verma* and Chengjun Liu

Department of Computer Science,
New Jersey Institute of Technology,
Newark, NJ 07102, USA
E-mail: av56@njit.edu
E-mail: chengjun.liu@njit.edu
*Corresponding author

Jiancheng (Kevin) Jia

Department of Test Engineering,
International Game Technology,
Reno, NV 89521, USA
E-mail: kevin.jia@igt.com

Abstract: A new iris recognition method based on a robust iris segmentation approach is presented in this paper for improving iris recognition performance. The robust iris segmentation approach applies power-law transformations for more accurate detection of the pupil region, which significantly reduces the candidate limbic boundary search space for increasing detection accuracy and efficiency. The limbic circle having a center within close range of the pupil center is selectively detected, and the eyelid detection approach thus leads to improved iris recognition performance. Experiments using the Iris Challenge Evaluation (ICE) database show the effectiveness of the proposed method.

Keywords: Iris recognition, iris segmentation, power-law transformations, Iris Challenge Evaluation (ICE).

Reference to this paper should be made as follows: A. Verma and C. Liu (xxxx) 'Iris recognition based on robust iris segmentation and image enhancement', *Int. J. Biometrics*, Vol. x, No. x, pp.xxx–xxx.

Biographical notes: Abhishek Verma received his Master of Computer Applications (MCA) degree from Bangalore University, Bangalore, India, in 2003, and MS in Computer Science from New Jersey Institute of Technology, NJ, USA, in 2006. He is currently working towards his Ph.D. degree in Computer Science at New Jersey Institute of Technology. His research interests include object and scene classification, pattern recognition, content-based image retrieval systems, image processing, iris recognition, and biometrics.

Chengjun Liu is an Associate Professor of computer science and the Director of the Face Recognition and Video Processing Lab at

New Jersey Institute of Technology (NJIT). He received his Ph.D. in computer science from George Mason University in 1999. From 1999 to 2001, he served on the faculty of University of Missouri - St. Louis. Since 2001, he has been on the faculty of NJIT, where he was promoted to Associate Professor with tenure in 2006. His research is in pattern recognition, machine learning, computer vision, image and video analysis, and security.

Jiancheng (Kevin) Jia received the M.S.E. and Ph.D. degrees from Purdue University in 1987 and 1991, respectively. He was a faculty member in the School of Electrical and Electronic Engineering at Nanyang Technological University, Singapore, from 1992 to 1997 and currently works at International Game Technology, USA. His research interests include biometrics, data representation with neural networks, pattern recognition and computer vision.

1 Introduction

Over the past decade biometric authentication has become a very active area of research due to the increasing demands in automated personal identification. More recently several new notable techniques and methods with applications to face recognition (Shih and Liu, 2011; Liu and Yang, 2009; Liu, 2007; Yang et al., 2010), eye detection (Shuo and Liu, 2010) and iris (Verma et al., 2011) biometrics have been proposed. Among many biometric techniques, iris recognition is one of the most promising approaches due to its high reliability for person identification (Ma et al., 2004).

The iris is a thin circular diaphragm, which lies between the lens and cornea of the human eye. Fig. 1 shows the iris region between the sclera and the pupil. The formation of the unique patterns of the iris is random and not related to any genetic factors (Wildes, 1997), and the iris patterns remain stable throughout the adult life. Thus, the patterns within the iris are unique to each person and two eyes of an individual have independent iris patterns. Some research shows that when compared with other biometric features such as face and fingerprint, iris patterns are more stable and reliable (Du et al., 2004).

In this paper, we propose a new iris recognition method based on a robust iris segmentation approach for improving iris recognition performance. We make major improvements in the iris segmentation phase. In particular, (i) we implement the power-law transformations for more accurate detection of the pupil region. Additionally, (ii) with our technique we are able to considerably reduce the candidate limbic boundary search space, this leads to a significant increase in the accuracy and speed of the segmentation. The segmentation performance is further enhanced with the application of thresholding. Furthermore, (iii) for higher accuracy and speed, we selectively detect the limbic circle having a center within close range of the pupil center. Additionally, (iv) our eyelid detection approach is shown to improve performance. The effectiveness of the proposed method is evaluated on a grand challenge, large scale database: the Iris Challenge Evaluation (ICE) (Phillips, 2006) dataset.

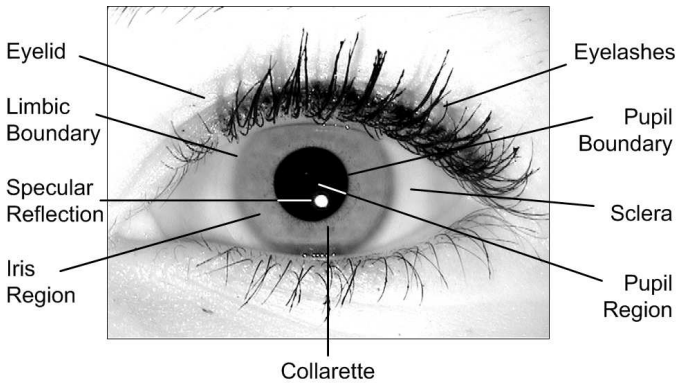

Figure 1 Front view of the human eye. The various parts labeled are important to iris segmentation and recognition.

Our method is able to correctly segment the pupil for 99.8% of the images in the dataset. Iris region detection is 98.5% for the right eye and 98.8% for the left eye. The rank-one recognition rate for our method is 3.5% and 2.7% higher than that of the irisBEE method (Phillips et al., 2008) for the right eye and the left eye respectively. Furthermore, we improve upon the ND_IRIS (Liu et al., 2005) by a significant 1.9% on the rank-one recognition rate for the left eye. The verification rate is about 10% higher than the irisBEE method (Phillips et al., 2008) for each eye at a much lower equal error rate; this emphasizes the higher accuracy of our method.

The rest of the paper is structured as follows: In Section 2, we briefly overview several representative works on image acquisition, segmentation, feature encoding and matching. Section 3 describes the dataset used in our experiments along with the implementation details of our improved recognition method. We evaluate the performance of our method and present a detailed analysis of the experimental results in Section 4 and conclusions are drawn in Section 5.

2 Related work

A general approach to iris recognition consists mainly of four stages: (1) image acquisition, (2) iris segmentation, (3) texture analysis, and (4) matching of texture patterns. Here we summarize several notable contributions to the aforementioned stages.

One of the earlier systems proposed by Flom and Safir (1987) detected the pupil region by finding large connected regions of pixels with intensity values below a given threshold. Iris descriptors were extracted using the difference operator, edge detection algorithms, and the Hough transform. Wildes (1997) system used low light level camera along with diffuse source and polarization for image acquisition. Iris region was segmented by computing the binary edge map followed by the Hough transform. For matching, it applied the Laplacian of Gaussian filter

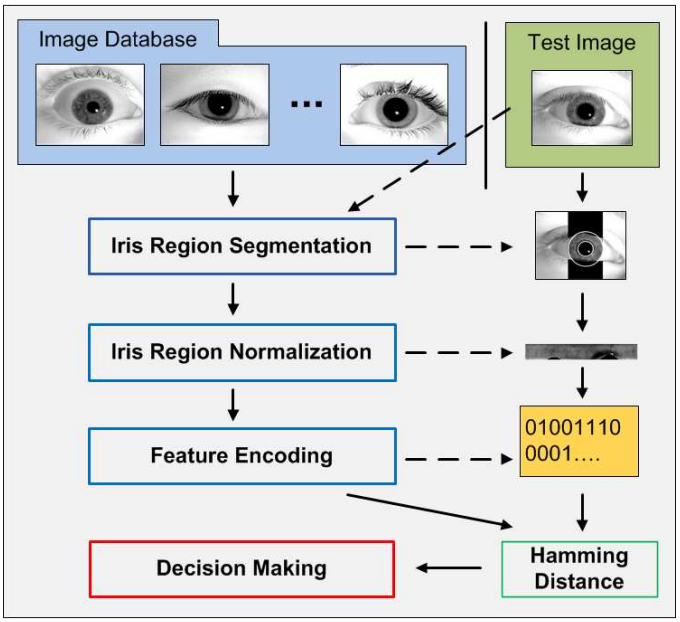

Figure 2 An overview of our iris recognition method.

at multiple scales to produce a template and computes the normalized correlation as a similarity measure.

Masek (2003) performed segmentation of iris by canny edge detection and circular Hough transform. Encoding was performed by 1D Log-Gabor wavelets and matching was based on hamming distance. Liu et al. (2005) proposed the ND_IRIS method based on Masek's implementation, hamming distance was used to compare two iris templates. The method proposed by Daugman (2006, 2007) performed segmentation of the iris region with the integro-differential operator followed by its normalization. The normalized iris image was convolved with the 2D Gabor filters to extract the texture information, which was quantized into a compact 256 byte binary iriscode. The iriscodes were compared using the normalized Hamming distance.

The issue of noise detection and handling for non-cooperative iris recognition was explored by Proenca (2006); Proenca and Luis (2007). Bayesian approach to matching of warped iris patterns was discussed by Thornton et al. (2007). More updated methods in image understanding for iris biometrics were reviewed by Bowyer et al. (2008). Vatsa et al. (2008) proposed a curve evolution approach to segment a non-ideal iris image using the modified Mumford-Shah functional. Beacon guided search for fast iris matching was discussed by Hao et al. (2008) and use of short-length iris codes from the most descriptive regions of the iris for fast matching was proposed by Gentile et al. (2009). He et al. (2009) proposed an Adaboost-cascade iris detector for fast iris segmentation. Spline based edge fitting scheme was used for non-circular iris boundary detection. Eyelashes and shadows were detected via a learned prediction model. Baker et al. (2010) explored the issue of degraded iris biometrics performance with non-cosmetic contact lenses. Proenca

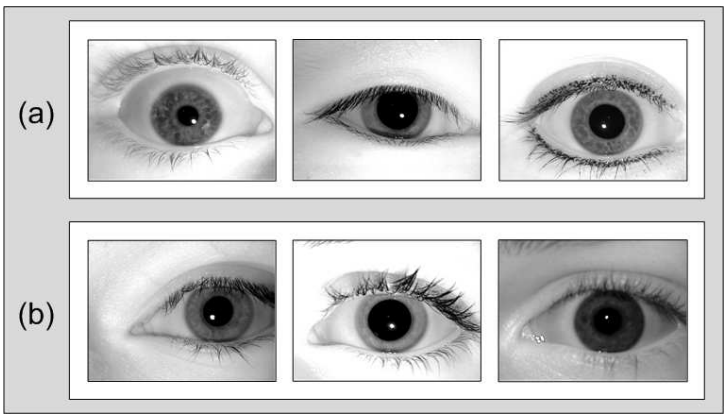

Figure 3 Example images of the (a) right eye and (b) left eye from the ICE dataset, under varying illumination levels, pupil dilation, angle and occlusion.

(2010) proposed a segmentation method to handle the degraded images acquired in less constrained conditions for real-time applications. Puhan et al. (2011) propose a fast iris segmentation technique based on the Fourier spectral density for noisy frontal view eye images captured with minimum cooperation from the subjects.

3 Robust iris recognition method and its major components

We propose and implement a robust iris recognition method and show the improvement in iris recognition performance using the Iris Challenge Evaluation (ICE) (Phillips, 2006) dataset. First we give details of the ICE dataset in Section 3.1. Next we discuss the major components of our iris recognition method. These include iris segmentation, iris encoding, and iris matching. See Fig. 2 for an overview of the iris recognition method.

We focus our efforts mainly on improving the iris segmentation stage of the system. This allows us to compare the performance of the segmentation stage with that implemented by the irisBEE method (Phillips et al., 2008). The segmentation step performs the localization of the iris region by detecting the pupil and the limbic boundary along with the eyelid detection. The iris encoding and iris matching stage are similar to that implemented by the irisBEE method (Phillips et al., 2008) in the Biometric Experimentation Environment (BEE) system. In comparison to the irisBEE method (Phillips et al., 2008) our proposed method leads to a significant increase in the accuracy of the iris region segmentation along with a much higher overall recognition performance at a lower error rate. Furthermore, our method outperforms the rank-one recognition performance achieved by the ND_IRIS (Liu et al., 2005) method.

3.1 The Iris Challenge Evaluation (ICE) dataset

The ICE dataset (Phillips, 2006) consists of 1425 right eye images of 124 different subjects and 1528 left eye images of 120 different subjects. Eye images belong to

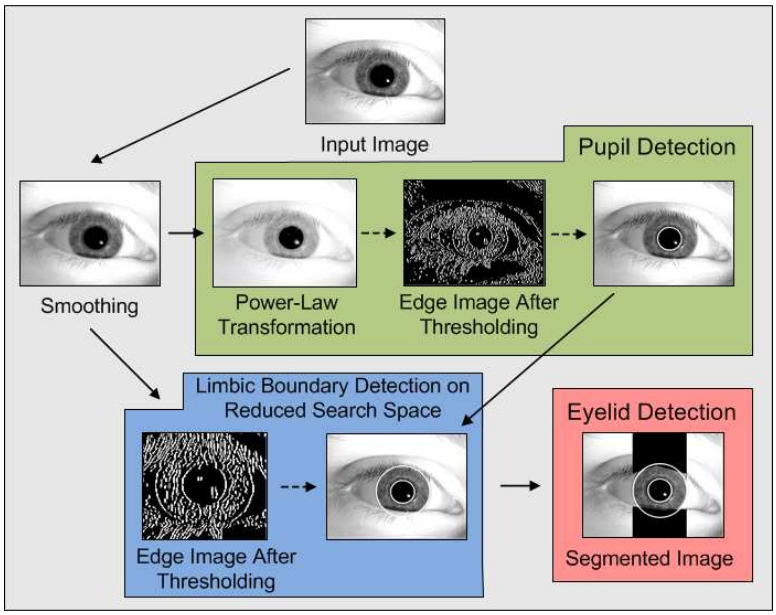

Figure 4 An overview of the three main stages in iris segmentation: the pupil detection, the limbic boundary detection, and the eyelid detection.

132 total subjects with 112 overlapping subjects between the left eye and the right eye images. The iris images are intensity images with a resolution of 640 x 480 in the TIFF format. The average diameter of an iris is 228 pixels. The images vary in quality due to the percentage of the iris region occlusion, the degree of blur in the image, off angle image, and images with subject wearing the contact lens. Fig. 3(a) shows some example images of the right eye and Fig. 3(b) shows some images from the left eye from the ICE dataset. Notice the varying degree of illumination levels, pupil dilation, angle and occlusion.

3.2 Iris segmentation

Here we give the details of our iris segmentation method. In particular, we discuss the effect of the power-law transformations on an eye image along with its advantages. Next we provide details of efficient determination of the pupil region, followed by a discussion on the effective method to determine the limbic boundary and the iris region segmentation. Finally, we give details of the improved eyelid detection phase. See Fig. 4 for an overview of the three main stages in iris segmentation: the pupil detection, the limbic boundary detection, and the eyelid detection.

3.2.1 Performing the power-law transformations on an eye image

The power-law transformation when applied to a grayscale image changes its dynamic range. The pixel intensity values in the input image act as the basis,

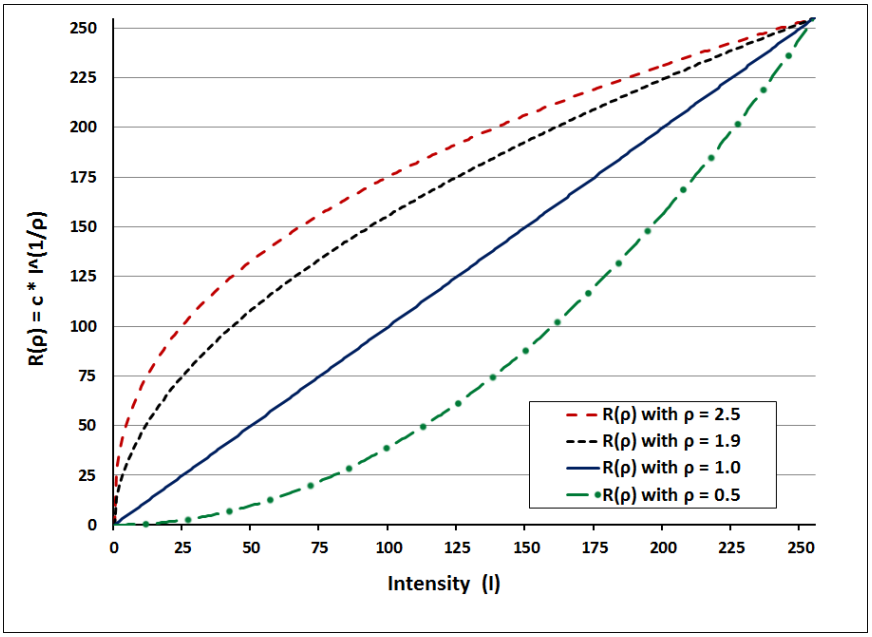

Figure 5 Plot showing the result of the power-law transformations on the image intensity values at various values of ρ.

which is raised to a (fixed) power. The operator is defined by the following formula (Gonzalez and Woods, 2001):

$$R(\rho) = c * I^{\frac{1}{\rho}} \tag{1}$$

where I is the intensity value of a pixel in the input image, c is the scaling factor, and $1/\rho$ is the power.

For $\rho < 1$, this operation increases the bandwidth of the high intensity values at the cost of the low pixel values. For $\rho > 1$, this process enhances the low intensity values while decreasing the bandwidth of the high intensity values, i.e., boosts the contrast in the dark regions. For $\rho = 1$, the above transformation linearly scales the intensity values.

In Fig. 5 the plot shows the result of the power-law transformations on the image intensity values at various values of ρ. The output pixel intensity value is scaled back to [0, 255]. This operation when applied on the input pixel intensity with $\rho = 1$ and $c = 1$ does not have any effect on the output intensity. This can be seen in the plot for $R(\rho)$ at $\rho = 1$. At $\rho = 1.9$ and 2.5 the lower intensity values gain more than the higher intensity values. At $\rho = 0.5$ the intensity values get pulled down and the lower values tend to get mapped into a narrower range.

We assess the impact of the power-law transformations on an eye image in terms of the pixel intensity frequency in Fig. 6. The original eye image is shown in Fig. 6(a), transformed images with ρ values as 0.5, 1.9 and 2.5 can be seen in Fig. 6(b), (c) and (d) respectively. The corresponding pixel intensity frequency plot for the four images is presented in Fig. 6(e). For $\rho > 1$ many more pixels get

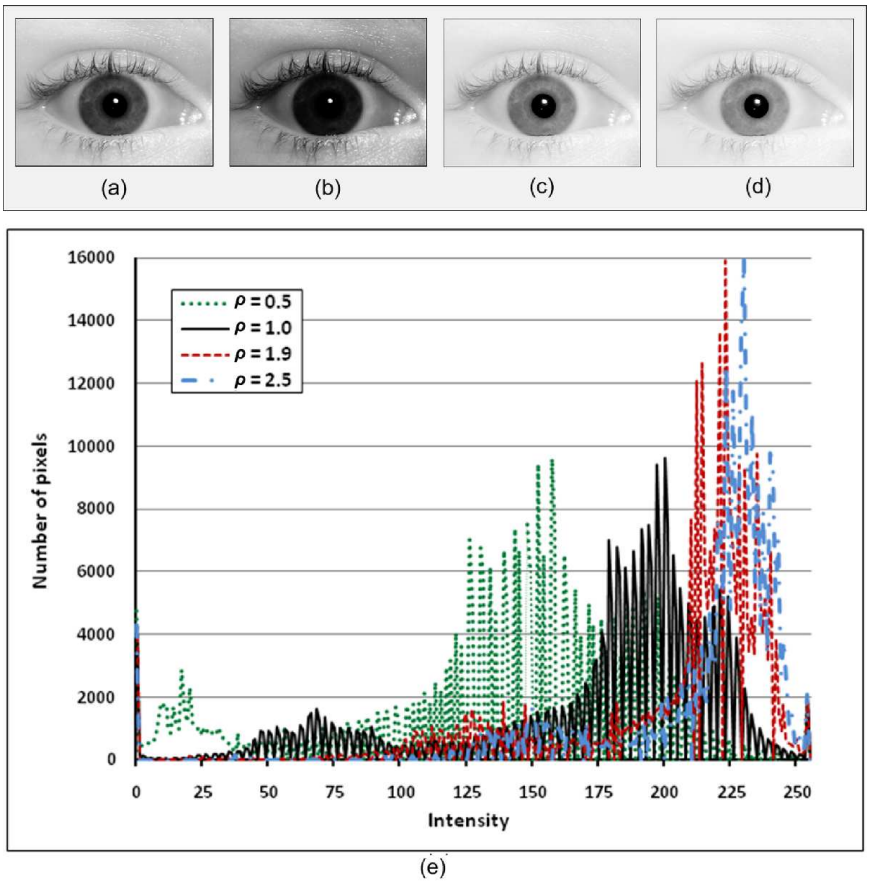

Figure 6 Results of the power-law transformations on (a) input eye image, at $\rho = 0.5$, 1.9 and 2.5 shown in (b), (c) and (d) respectively. (e) Plot of the frequency of intensity of the input image at various ρ values. Plot at $\rho = 1.0$ corresponds to the input image in (a).

mapped into a narrower brighter intensity range as seen in Fig. 6(e). Also, this effect can be observed from the eye images in Fig. 6(c) and (d) where the contrast between the pupil and the iris becomes more significant.

3.2.2 Efficient determination of the pupil region

Our new iris segmentation method first applies the power-law transformation on an eye image and then detects the pupil boundary. We first detect the pupil boundary and then detect the outer iris boundary. The reason for this approach lies in the observation that the contrast between the iris and the pupil is usually larger than that between the iris and the sclera. The contrast is further enhanced from the application of the power-law transformation; this makes it easier to detect the pupil region and thereby increases the accuracy of the pupil segmentation. Our method results in the accurate detection of the pupil boundary for 99.8% of the

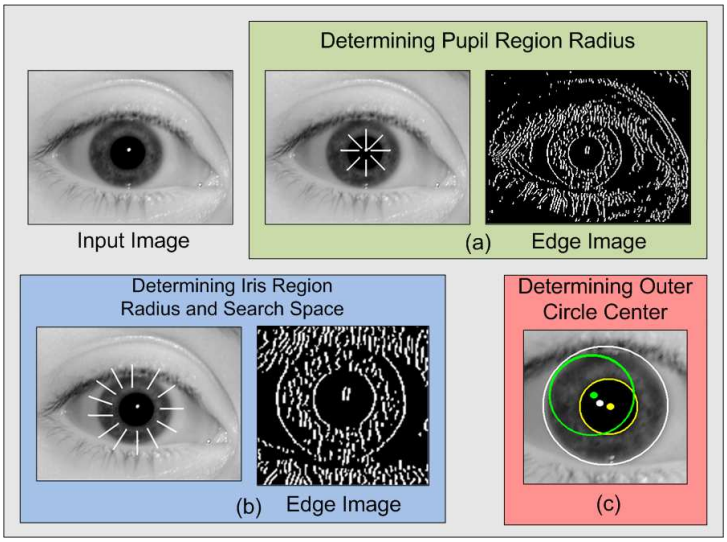

Figure 7 Efficient determination of: (a) the pupil region radius, (b) the iris region radius and search space, and (c) the limbic boundary center.

images in the dataset; this includes all the right eye and the left eye images. The appropriate ρ value for the power-law transformation is selected after analyzing the contrast between the iris and the pupil on a validation set chosen from the ICE dataset.

In Fig. 4 and Fig. 7(a) we present the details of the pupil detection. In order to get rid of the noise, as a first step we apply the Gaussian filter to smooth the input image. The Gaussian smoothing filter is defined by the following formula (Forsyth and Ponce, 2003):

$$G(x,y) = \frac{1}{2\pi\sigma^2} e^{-\frac{x^2+y^2}{2\sigma^2}} \tag{2}$$

where x is the distance from the origin in the horizontal axis, y is the distance from the origin in the vertical axis, and σ is the standard deviation of the Gaussian distribution. In the next stage, we apply the power-law transformation followed by the canny edge detector to detect edges in the image. Thresholding is performed to get rid of the weak edges.

Finally, we apply the circular Hough transform on the edge image to detect the pupil boundary. In order to make the pupil search more accurate and fast, we search for a candidate pupil having radius within a narrow range. This range is computed from a validation set chosen from the ICE dataset. See in Fig. 7(a) the image on the left for the range of the radius and on the right the edge image space to be searched for candidate pupil circles. The circular Hough transform can be described as a transformation of a point in the x, y-plane to the circle parameter space. The parametric representation of the circle is given as:

$$\begin{aligned} x &= a + r\cos(\theta) \\ y &= b + r\sin(\theta) \end{aligned} \tag{3}$$

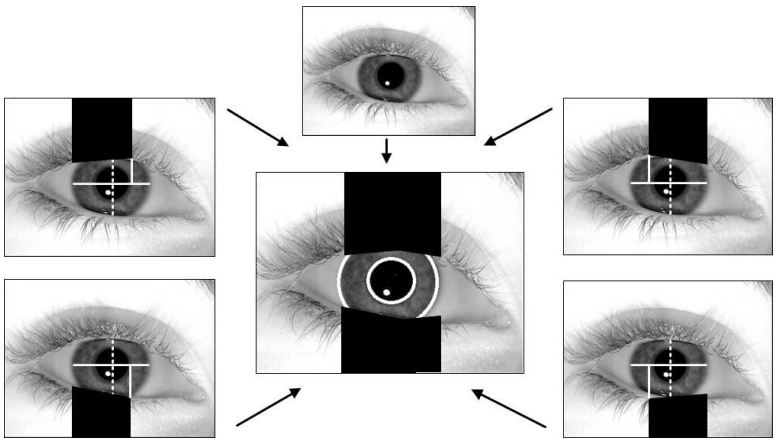

Figure 8 Detection of iris region occlusion from the upper and lower eyelid.

where a and b are the center of the circle in the x and y direction respectively and where r is the radius and θ is the angle between 0 and 2π.

3.2.3 Efficient determination of the limbic boundary and the iris region

We observe that when detecting the limbic boundary the Hough transform often makes incorrect detections. Our research reveals that such incorrect detections are due to the presence of a large number of weak edges. Therefore, we apply a thresholding technique on the edge image produced by the Canny edge detector to get rid of the insignificant edge points. This has shown to improve the percentage of the correctly segmented iris region by close to 3% for both the right eye and the left eye images. See Fig. 4 and Fig. 7(b) for details.

In order to further improve the accuracy of the Hough transform for detecting the limbic boundary, we search for the circle within a specific region around the detected pupil boundary. Furthermore, we search for a candidate limbic boundary having radius within a narrow range. The range for the radius is estimated on the validation set chosen from the ICE dataset. The reduced search space and the narrow radius range thus considerably increase the speed of the circle detection. See in Fig. 7(b) the image on the left for the range of the radius and on the right the reduced edge image space that is searched for candidate limbic circles.

Additionally, we apply another efficient technique to detect the limbic boundary. The Hough transform implemented by the irisBEE method (Phillips et al., 2008) searches the maximum in the parameter space to detect the circle. We implement a technique based on the Hough transform that increases the accuracy of the correct limbic boundary detection by 1.3% for the right eye and by 1.4% for the left eye images. Specifically, when the distance between the center of the detected circle and the center of the detected pupil is more than a predefined threshold value, then the detected circle is rejected. Out of all the non-rejected circles we select the one that corresponds to the maximum in the parameter space of the Hough transform and has center coordinates within a predefined threshold value from the pupil center. As a result, our heuristic method

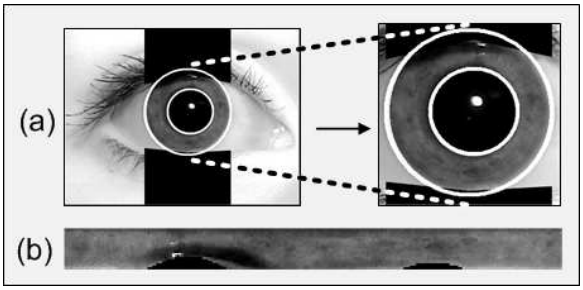

Figure 9 (a) Segmented iris region and (b) its normalized iris region.

considerably increases the accuracy of the Hough transform. In Fig. 7(c) the center of the pupil is pointed in yellow, the incorrect limbic boundary circle with center in green is rejected as it is farther away from the pupil center when compared to the acceptable limbic detection with center displayed in white.

Here we present the results of time complexity analysis for the segmentation stage. We compute the mean average implementation time of the segmentation stage for an image. First we compute the average processing time for an image from all 2953 images and then perform ten runs to obtain the mean average implementation time for an image. The experiment is performed on a 3.00 GHz Pentium 4 CPU with 3.2 GB RAM running on Linux. By reducing the search space for Hough transform our algorithm takes 748 milliseconds to process an image against 853 milliseconds without this optimization. Hence, our efficient limbic boundary detection technique decreases the processing time by approximately 12%.

3.2.4 Improved eyelid detection

One of the earlier system proposed by Wildes (1997) detects the eyelids by applying edge detection filter and Hough transform to obtain edge points and then fits parameterized parabolic arcs to localize the upper and lower eyelids. We implement the eyelid detection by modeling the eyelid as two straight lines using linear Hough transform. Additionaly, we perform power-law transformation on an eye image in order to enhance the contrast between the eyelid and the iris/pupil region. Hence, we are able to more accurately detect the occlusion from eyelids.

Furthermore, we split the iris region horizontally and vertically resulting in four windows. See Fig. 8 for the result of eyelid detection. In order to detect the upper eyelid we search within the top half of the iris region. Furthermore, to detect the top left of the eyelid region, we consider only the left three quarters of the top half of the iris region. The top right of the eyelid region is detected within the right three quarters of the top half of the iris region. Thus, there is an overlap of a portion of the iris region between two splits. Similarly, we detect the bottom eyelid in the lower two windows. After detecting the eyelid in each of these four windows we connect the results together. Our approach has shown to improve performance when compared to the method in (Liu et al., 2005) where the splits do not overlap.

Table 1 Correctness of Segmentation (in percentage %) for the Pupil and Iris Region at Various Values of ρ

ρ	Right Eye		Left Eye	
	Pupil Region	Iris Region	Pupil Region	Iris Region
0.7	96.3	95.5	96.8	96.0
1.0	98.3	97.4	98.6	97.7
1.3	98.9	98.0	99.2	98.1
1.6	99.2	98.2	99.5	98.4
1.9	**99.7**	**98.5**	**99.9**	**98.8**
2.2	99.6	98.4	99.9	98.8
2.5	99.6	98.4	99.8	98.7

3.3 Feature encoding and matching

The feature encoding stage encodes the iris image texture patterns into iriscodes using filters. We normalize the iris region to a constant dimension before encoding. Denoising of the noise regions in the normalized pattern is implemented by means of averaging. This results in a bitwise template, which contains iris information and a noise mask for corrupt areas within the iris pattern. Fig. 9 shows the result of the normalization of the iris region.

Encoding is implemented by convolving the normalized iris pattern with the 1D Log-Gabor wavelets (Masek, 2003). The frequency response of a Log-Gabor filter is given as:

$$G(f) = \exp\left(\frac{-(\log(f/f_0))^2}{2(\log(\sigma/f_0))^2}\right) \tag{4}$$

where f_0 represents the centre frequency, and σ gives the bandwidth of the filter. Details of the Log-Gabor filter are given by Field (1987).

We use the Hamming distance to measure the similarity of the two iris templates. The Hamming distance defines the similarity between two iriscodes, and the two iriscodes are a match when their Hamming distance is close to each other. In comparing the bit patterns X and Y, the Hamming distance (HD) is defined as the sum of disagreeing bits (sum of the XOR between X and Y) over N, which is the total number of bits in the bit pattern. Below is the formula:

$$\text{HD}= \frac{1}{N}\sum_{j=1}^{N} X_j \oplus Y_j \tag{5}$$

Noise bits in the two templates are discarded. The iris template is shifted bit-wise from -15 degrees to +15 degrees with an increment of 1.5 degrees each time, and the Hamming distance is computed for two shift positions. The lowest Hamming distance is the best match between the two templates. As suggested by Daugman (2002) such shifting is necessary to take care of the misalignment in the normalized iris patterns caused by the rotational differences during imaging.

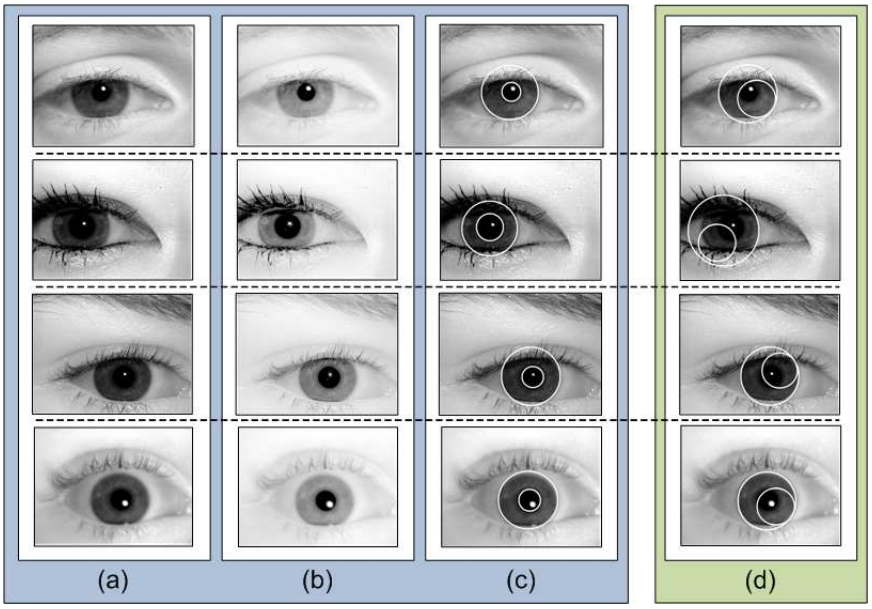

Figure 10 Comparison of the pupil segmentation performance of our improved method with the irisBEE method (Phillips et al., 2008). (a) Input eye images, (b) images after the power-law transformation, (c) examples of correct segmentation of the pupil and iris region by our method, and (d) examples of incorrect segmentation by the irisBEE method (Phillips et al., 2008).

4 Experimental results

Here we present the details of the experimental evaluation of our proposed method on the ICE dataset. In order for us to make a through comparative assessment of the performance of our method with other methods, we conduct three sets of experiments for the right eye and the left eye. First we assess the correctness of iris segmentation, next we assess the rank-one recognition performance and finally we assess the verification performance for the right eye and the left eye according to the experimental setup proposed by the ICE system. The rank-one recognition criterion and the verification criterion evaluate the performance of our method for recognition from two different viewpoints; we provide more details later in this Section. For all our experiments we scale the input image to 0.4 of its original size, this significantly cuts down the processing time without compromising the correctness of the results.

4.1 Assessing the correctness of segmentation

The first set of experiments are designed to assess the correctness of segmentation for the pupil region, the limbic boundary and the iris region on the right eye and the left eye. Considering the nature of the ICE dataset, we now define the correctness of segmentation based on the assumption that the pupil and iris can be modeled as a circle. The pupil region is said to be correctly segmented when

Table 2 Comparison with the Results (in percentage %) from the irisBEE Method (Phillips et al., 2008) of the Correctness of Segmentation for the Pupil Region, Limbic Boundary and Iris Region

Regions	Our Method		irisBEE Method	
	Right Eye	Left Eye	Right Eye	Left Eye
Pupil Region	**99.7**	**99.9**	95.4	95.7
Limbic Boundary	**98.7**	**99.0**	93.4	93.6
Iris Region	**98.5**	**98.8**	90.2	90.5

the circle fully encloses the pupil region and does not include any area other than the dark pupil. Incorrect pupil segmentation may cover parts of the iris region and or only enclose the pupil region partially. Refer to Section 3.2.2 for the discussion on the method and Fig. 10(c) and (d) for the results. The limbic boundary is said to be correctly segmented when the circle fully bounds the iris region from outside and does not include any area outside of the iris region other than the pupil or the eyelids that may sometimes occlude the iris. Incorrect limbic boundary segmentation may cover parts of the sclera region and or only enclose the iris region partially. Refer to Section 3.2.3 for the discussion on the method and Fig. 11(a) and (b) for the results. The iris region is said to be correctly segmented when for any given eye image both the pupil and the limbic boundary are correctly detected.

In Table 1 we give the results of the correctness of the pupil and iris region segmentation. The power-law transformations are performed for pupil detection on the right and left eye image at various values of ρ. At $\rho = 1$ and $c = 1$ the power-law transformation leaves the intensity values of the pixels in the input image unchanged. For values of $\rho > 1$, the power-law transformation enhances the contrast in the dark regions and thereby makes the pupil boundary easier to detect. This is confirmed by the percentage of correct pupil detection as ρ goes higher. Also, for $\rho < 1$, the contrast between the pupil and the surrounding region decreases making it harder to detect the pupil. We obtain best pupil detection results at $\rho = 1.9$ with close to 100% correct pupil detection for the left eye and 99.7% for the right eye. For the ρ values higher than 1.9, we do not notice any significant change in the segmentation performance. The best result for the iris region detection is 98.5% for the right eye and 98.8% for the left eye. The iris region detection is at its highest when the pupil region detection is at its maximum; this is largely due to the fact that for our method the correct detection of iris region is to an extent dependent on the correct pupil region detection. Finally, the iris region detection rate at $\rho = 1.9$ is 1.1% higher for both the right and the left eye when compared with the rate at $\rho = 1$.

Fig. 10(c) shows examples of correct segmentation of the pupil based on our improved pupil region detection method. Input images are shown in Fig. 10(a) and the result of the power-law transformation can be seen from Fig. 10(b). We compare our results to the incorrect segmentation results of the irisBEE method (Phillips et al., 2008) in Fig. 10(d). In Fig. 11(a) we present the results of our improved limbic boundary segmentation method and make a comparison with the

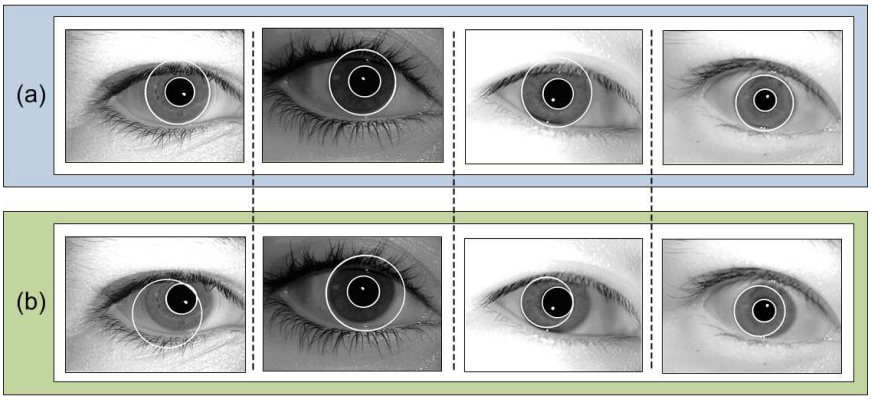

Figure 11 Comparison of the limbic boundary segmentation performance of our improved method with the irisBEE method (Phillips et al., 2008). (a) Examples of correct segmentation by our method and (b) examples of incorrect segmentation by the irisBEE method (Phillips et al., 2008).

Table 3 Rank-one Recognition Performance (in percentage %) at Various Values of ρ

ρ	Right Eye	Left Eye
0.7	95.4	95.9
1.0	97.6	98.1
1.3	98.3	98.5
1.6	98.7	98.8
1.9	**99.0**	**99.0**
2.2	98.9	99.0
2.5	98.9	98.9

incorrect limbic boundary detections of the irisBEE method (Phillips et al., 2008) shown in Fig. 11(b).

From Table 2 it can be seen that our method improves upon the irisBEE method (Phillips et al., 2008) for pupil region segmentation by 4.3% and 4.2% for the right eye and the left eye respectively. Our limbic boundary detection rates are higher by 5.3% and 5.4% for the right and left eye respectively. Finally, we improve upon the irisBEE method (Phillips et al., 2008) by 8.3% for both the right and the left eye iris region detection.

4.2 Assessment of the rank-one recognition performance

Here we evaluate the effectiveness of our method based on the rank-one recognition rate. This is a popular evaluation criterion for iris recognition. In order to obtain the recognition rate, we need to first calculate the Hamming distance between every pair of a query image and a target image, and then use the nearest-neighbor classifier for classifying all query images. If the query image and the target image belong to the same subject, then it is considered as a correct match.

Table 4 Comparison of the Rank-one Recognition Performance (in percentage %) with the Other Methods

Methods	Right Eye	Left Eye
Our Method	**99.0**	**99.0**
ND_IRIS (Liu et al., 2005)	-	97.1
irisBEE method (Phillips et al., 2008)	95.5	96.3

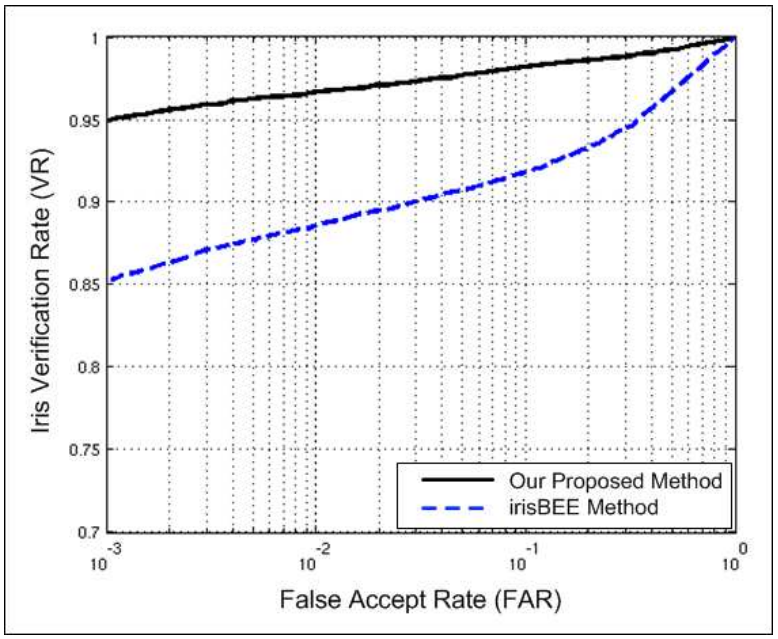

Figure 12 Comparison of the iris verification performance (ROC curve for the right eye) of the irisBEE method (Phillips et al., 2008) with our proposed method.

The recognition rate is the ratio of the number of correctly classified query images to the total number of query images. The rank-one recognition rate underlines the similarity of the samples that are close to one another within a class.

From Table 3 it can be seen that the best recognition rate is 99% for both the right eye and the left eye at $\rho = 1.9$, when compared to the rate at $\rho = 1$, this is higher by 1.4% for the right eye and by 0.9% for the left eye. We do not notice any significant change in the recognition performance for $\rho > 1.9$.

The rank-one recognition rate for our method as shown in Table 4 is 3.5% and 2.7% higher than that of the irisBEE method (Phillips et al., 2008) for the right eye and the left eye respectively. Furthermore, we improve upon the ND_IRIS (Liu et al., 2005) by a significant 1.9% for the left eye. Note that the authors in (Liu et al., 2005) do not report the recognition rate on the right eye. Additionally, our improved eyelid detection method as decribed in Section 3.2.4 contributes to a performance increase of 1% for both the right and the left eye.

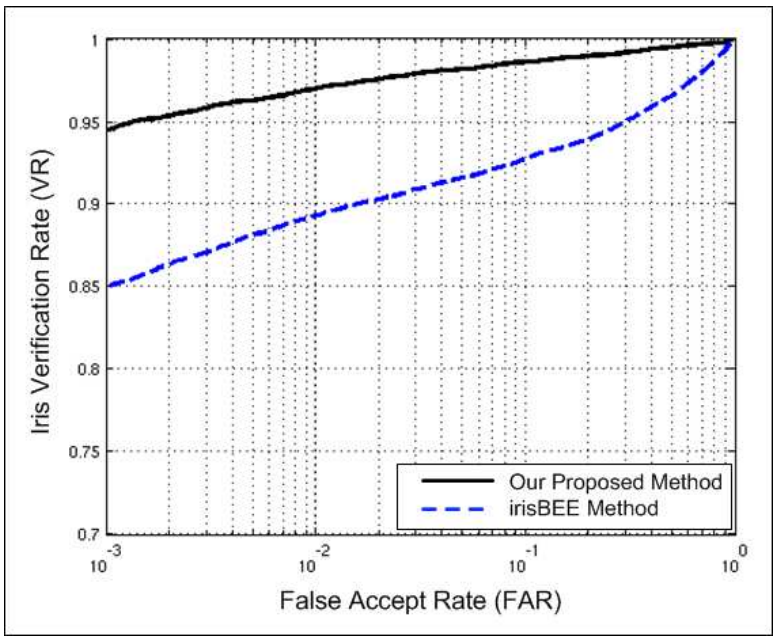

Figure 13 Comparison of the iris verification performance (ROC curve for the left eye) of the irisBEE method (Phillips et al., 2008) with our proposed method.

4.3 Assessment of the verification performance and equal error rate (EER)

In our final set of experiments we evaluate the verification performance and compare our results with the irisBEE method (Phillips et al., 2008). The ICE protocol recommends using the receiver operating characteristic (ROC) curves, which plot the iris verification rate, i.e., the true accept rate versus the false accept rate (FAR), to report the iris recognition performance. The verification rate is the rate at which a matching algorithm correctly determines that a genuine sample matches an enrolled sample. The equal error rate (EER) is obtained when the FAR equals the false reject rate (FRR). Generally, the lower the EER value the higher will be the accuracy of the biometric system.

The ROC curves are automatically generated by the BEE system when a similarity matrix is input to the system. In particular, the BEE system generates two ROC curves, corresponding to the Experiment 1 for the right eye and Experiment 2 for the left eye images. The iris verification rate at the false accept rate of 0.1% is generally used as a standard for performance comparison (Yang et al., 2010).

It should be pointed out that the verification rate in the ICE Experiment 1 and 2 emphasizes the similarity of samples that are relatively distant from one another within a class because it needs to measure all similarity between samples, whereas the recognition rate discussed in Section 4.2 emphasizes the similarity of samples that are close to one another within a class since it applies a nearest-neighbor

Table 5 Iris Verification Performance (in percentage %) at 0.1% False Accept Rate and EER at Various Values of ρ (VR is the verification rate and EER is the equal error rate.)

ρ	Right Eye		Left Eye	
	VR	EER	VR	EER
0.7	85.1	8.3	84.7	7.7
1.0	91.3	5.2	90.9	4.6
1.3	92.8	4.9	92.2	4.2
1.6	94.2	3.9	93.3	3.1
1.9	**95.1**	**2.8**	**94.4**	**2.3**
2.2	95.1	2.8	94.4	2.3
2.5	95.0	2.8	94.3	2.3

Table 6 Comparison with other Methods on the Iris Verification Performance (in percentage %) at 0.1% False Accept Rate and EER (VR is the verification rate and EER is the equal error rate.)

Methods	Right Eye		Left Eye	
	VR	EER	VR	EER
Our Method	95.1	**2.8**	94.4	**2.3**
SAGEM-Iridian†	above 99.0*	-	above 99.0*	-
irisBEE Method†	85.2	8.5	84.9	7.8

†Phillips et al. (2008). *Result estimated from Fig. 4 in Phillips et al. (2008).

classifier. Therefore, these two criteria evaluate the performance of our method for recognition from two different viewpoints.

From Table 5 it can be seen that the best verification rate and the lowest EER is achieved at $\rho = 1.9$. When compared to the performance at $\rho = 1$, the VR is higher by 3.8% at a low EER of 2.8% for the right eye and the VR is higher by 3.5% at the EER of 2.3% for the left eye. We do not notice any significant change in the verification performance for $\rho > 1.9$.

We compare in Fig. 12 and Fig. 13 the performance of our method with that of the irisBEE method (Phillips et al., 2008) in terms of the ROC curves. Fig. 12 and Fig. 13 show the ROC curves for the right eye experiment and the left eye experiment respectively. It can be observed that our proposed method improves the iris recognition performance significantly in comparison with the irisBEE method (Phillips et al., 2008).

From Table 6 it can be seen that our method improves upon the irisBEE method (Phillips et al., 2008) notably. For the right eye, our proposed method has a verification rate of 95.1%, which is about 10% higher than the irisBEE method (Phillips et al., 2008). The EER is 2.8%, which is much lower than the 8.5% for the irisBEE method (Phillips et al., 2008). For the left eye, our proposed method has a VR of 94.4%, which is again higher by 9.5% than the irisBEE method (Phillips et al., 2008). The EER is 2.3%, which is much lower than the 7.8% from the

irisBEE method (Phillips et al., 2008); this emphasizes the higher accuracy of our method.

5 Conclusion

In this paper, we presented a robust iris recognition method with enhanced performance on the ICE dataset. In particular, we implemented the power-law transformations for more accurate detection of the pupil region. Additionally, with our technique we are able to considerably reduce the candidate limbic boundary search space, this leads to a significant increase in the accuracy and speed of the segmentation. The segmentation performance is further increased with the application of the thresholding. Furthermore, for higher accuracy and speed, we selectively detect the limbic circle having a center within close range of the pupil center. Additionally, our improved eyelid detection phase has shown to increase performance. From the experiments, we can conclude that, using power-law transformations with $\rho = 1.9$ or above, our proposed method showed constantly better performance for pupil and iris region segmentation for both left and right eyes using the ICE dataset (Table 1), consequently comparison studies showed improved segmentation performance comparing with the irisBEE method (Phillips et al., 2008) (Table 2) and on the rank-one recognition performance than other methods (Table 4) with improved VR and EER (Table 6) for both eyes.

Note that the visible wavelength iris images, such as those in the UBIRIS database (Proenca et al., 2010), display different characteristics from the IR or near IR iris images in the ICE database. On the one hand, the visible wavelength iris images possess additional classification cues, such as color. But on the other hand, they pose challenging issues as well, such as large variations in lighting conditions. Our future work will leverage our research results in attenuating illumination variations (Liu, 2006), (Yang and Liu, 2007), applying novel color models (Liu and Liu, 2008b), (Liu and Liu, 2008a), (Yang and Liu, 2008), (Liu, 2008), as well as effective feature extraction and classification techniques (Liu and Wechsler, 2001), (Liu and Wechsler, 1998a), (Liu and Wechsler, 1998b) to process the visible wavelength iris images.

Acknowledgments:

The authors would like to thank the anonymous reviewers for their critical and constructive comments and suggestions.

References

S. Baker, A. Hentz, K. Bowyer, and P. Flynn. Degradation of iris recognition performance due to non-cosmetic prescription contact lenses. *Computer Vision and Image Understanding*, 114(9):1030–1044, 2010.

K.W. Bowyer, K. Hollingsworth, and P.J. Flynn. Image understanding for iris biometrics: A survey. *Computer Vision Image Understanding*, 110(2):281–307, 2008.

J. Daugman. How iris recognition works. In *IEEE Int. Conf. on Image Processing*, Rochester, New York, September 22-25 2002.

J. Daugman. Probing the uniqueness and randomness of iriscodes: Results from 200 billion iris pair comparisons. *Proc. of the IEEE*, 94(11):1927–1935, 2006.

J. Daugman. New methods in iris recognition. *IEEE Trans. on Systems, Man and Cybernetics B*, 37(5):1167–1175, 2007.

Y. Du, R.W. Ives, and D.M. Etter. Iris recognition: A chapter on biometrics. In *The Electrical Engineering Handbook*. CRC Press, Florida, 2004.

D.J. Field. Relations between the statistics of natural images and the response properties of cortical cells. *Journal of the Optical Society of America*, 12(4):2379–2394, 1987.

L. Flom and A. Safir. Iris recognition system. *U.S. Patent 4,641,349*, 1987.

D. Forsyth and J. Ponce. *Computer Vision: A Modern Approach*. Prentice Hall, NJ, 2003.

J.E. Gentile, N. Ratha, and J. Connell. SLIC: Short length iris code. In *Int. Conf. on Biometrics: Theory, Applications and Systems*, Washington, D.C., September 28-30 2009.

C.G. Gonzalez and R.E. Woods. *Digital Image Processing*. Prentice Hall, Upper Saddle River, NJ, USA, 2001.

F. Hao, J. Daugman, and P. Zielinski. A fast search algorithm for a large fuzzy database. *IEEE Trans. on Information Forensics and Security*, 2(3):203–212, 2008.

Z. He, T. Tan, Z. Sun, and X. Qiu. Toward accurate and fast iris segmentation for iris biometrics. *IEEE Trans. on Pattern Analysis and Machine Intelligence*, 31(9): 1670–1684, 2009.

C. Liu. Capitalize on dimensionality increasing techniques for improving face recognition grand challenge performance. *IEEE Trans. Pattern Analysis and Machine Intelligence*, 28(5):725–737, 2006.

C. Liu. The Bayes decision rule induced similarity measures. *IEEE Trans. on Pattern Analysis and Machine Intelligence*, 6(29):1116–1117, 2007.

C. Liu. Learning the uncorrelated, independent, and discriminating color spaces for face recognition. *IEEE Trans. on Information Forensics and Security*, 3(2):213–222, 2008.

C. Liu and H. Wechsler. Probabilistic reasoning models for face recognition. In *Proc. Computer Vision and Pattern Recognition*, pages 827–832, Santa Barbara, CA, June 23-25 1998a.

C. Liu and H. Wechsler. Unified Bayesian framework for face recognition. In *Proc. IEEE Int. Conf. on Image Processing*, pages 151–155, Chicago, IL, October 4-7 1998b.

C. Liu and H. Wechsler. A shape and texture based enhanced Fisher classifier for face recognition. *IEEE Trans. on Image Processing*, 10(4):598–608, 2001.

C. Liu and J. Yang. ICA color space for pattern recognition. *IEEE Trans. on Neural Networks*, 2(20):248–257, 2009.

X. Liu, K.W. Bowyer, and P.J. Flynn. Experiments with an improved iris segmentation algorithm. In *IEEE Workshop on Automatic Identification Advanced Technologies*, New York, October 16-18 2005.

Z. Liu and C. Liu. Fusion of the complementary discrete cosine features in the YIQ color space for face recognition. *Computer Vision and Image Understanding*, 111(3): 249262, 2008a.

Z. Liu and C. Liu. A hybrid color and frequency features method for face recognition. *IEEE Trans. on Image Processing*, 17(10):1975–1980, 2008b.

L. Ma, T. Tan, Y. Wang, and D. Zhang. Efficient iris recognition by characterizing key local variations. *IEEE Trans. Image Processing*, 13(6):739–750, 2004.

L. Masek. Recognition of human iris patterns for biometric identification. B. Eng. thesis, The University of Western Australia, Western Australia, 2003.

P.J. Phillips. FRGC and ICE workshop. Technical report, National Institute of Standards and Technology (NIST), USA, 2006.

P.J. Phillips, K.W. Bowyer, P.J. Flynn, X. Liu, and W.T. Scruggs. The iris challenge evaluation 2005. In *IEEE Second Int. Conf. on Biometrics: Theory, Applications and Systems*, Washington, D.C., September 29 - October 1 2008.

H. Proenca. *Towards Non-Cooperative Biometric Iris Recognition*. PhD thesis, University of Beira Interior, Covilha, Portugal, October 2006.

H. Proenca. Iris recognition: On the segmentation of degraded images acquired in the visible wavelength. *IEEE Trans. on Pattern Analysis and Machine Intelligence*, 32 (8):1502–1516, 2010.

H. Proenca, S. Filipe, R. Santos, J. Oliveira, and L.A. Alexandre. The UBIRIS.v2: A database of visible wavelength images captured on-the-move and at-a-distance. *IEEE Trans. Pattern Analysis and Machine Intelligence*, 32(8):1529–1535, 2010.

H. Proenca and A. Luis. Toward noncooperative iris recognition: A classification approach using multiple signatures. *IEEE Trans. on Pattern Analysis and Machine Intelligence*, 29:607–612, 2007.

N.B. Puhan, N. Sudha, and S.K. Anirudh. Efficient segmentation technique for noisy frontal view iris images using Fourier spectral density. *Signal Image and Video Processing*, 5(1):105–119, 2011.

P. Shih and C. Liu. An effective color feature extraction method using evolutionary computation for face recognition. *Int. Journal of Biometrics*, 2011. (to appear).

C. Shuo and C. Liu. Eye detection using color information and a new efficient SVM. In *Int. Conf. on Biometrics Theory, Applications and Systems*, Washington, D.C., September 27-29 2010.

J. Thornton, M. Savvides, and B.V.K. Vijayakumar. A bayesian approach to deformed pattern matching of iris images. *IEEE Trans. on Pattern Analysis and Machine Intelligence*, 4(29):596–606, 2007.

M. Vatsa, R. Singh, and A. Noore. Improving iris recognition performance using segmentation, quality enhancement, match score fusion, and indexing. *IEEE Trans. on Systems, Man, and Cybernetics - Part B: Cybernetics*, 38(4):1021–1035, 2008.

A. Verma, C. Liu, and J. Jia. New color SIFT descriptors for image classification with applications to biometrics. *Int. Journal of Biometrics*, 1(3):56–75, 2011.

R.P. Wildes. Iris recognition: An emerging biometric technology. *Proc. of the IEEE*, 85 (9):1348–1363, 1997.

J. Yang and C. Liu. Horizontal and vertical 2DPCA-based discriminant analysis for face verification on a large-scale database. *IEEE Trans. on Information Forensics and Security*, 2(4):781–792, 2007.

J. Yang and C. Liu. Color image discriminant models and algorithms for face recognition. *IEEE Trans. on Neural Networks*, 19(12):20882098, 2008.

J. Yang, C. Liu, and L. Zhang. Color space normalization: Enhancing the discriminating power of color spaces for face recognition. *Pattern Recognition*, 4(43):1454–1466, 2010.